Photodissociation of 1,3,5-Triazine: An Ab Initio and RRKM Study†

Y. A. Dyakov,*,‡ A. M. Mebel,*,§ S. H. Lin,‡,|| Y. T. Lee,‡,⊥ and C.-K. Ni‡,#

Institute of Atomic and Molecular Sciences, Academia Sinica, P.O. Box 23-166, Taipei 10764, Taiwan, Department of Chemistry and Biochemistry, Florida International University, 11200 SW 8th Street, Miami, Florida 33176, Department of Applied Chemistry, National Chiao-Tung University, Hsin-chu, Taiwan, Chemistry Department, National Taiwan University, Taipei, Taiwan, and Department of Chemistry, National Tsing Hua University, Hsinchu, Taiwan

Received: May 25, 2007

The ab initio/Rice−Ramsperger−Kassel−Marcus (RRKM) approach has been applied to investigate the photodissociation mechanism of 1,3,5-triazine at different wavelengths of the absorbed photon. Reaction pathways leading to various decomposition products have been mapped out at the G3(MP2,CC)//B3LYP level, and then the RRKM and microcanonical variational transition state theories have been applied to compute rate constants for individual reaction steps. Relative product yields (branching ratios) for the dissociation products have been calculated using the steady-state approach. The results show that, after being excited by 275, 248, or 193 nm photons, the triazine molecule isomerizes to an opened-ring structure on the first singlet excited-state potential energy surface (PES), which is followed by relaxation into the ground electronic state via internal conversion. On the contrary, excitation by 285 and 295 nm photons cannot initiate the ring-opening reaction on the excited-state PES, and the molecule relaxes into the energized ring isomer in the ground electronic state. The dissociation reaction starting from the ring isomer is calculated to have branching ratios of various reaction channels significantly different from those for the reaction initiating from the opened-ring structure. The existence of two distinct mechanisms of 1,3,5-triazine photodissociation can explain the inconsistency in the translational energy distributions of HCN moieties at different wavelengths observed experimentally.

1. Introduction

Photodissociation chemistry of 1,3,5-triazine ($C_3H_3N_3$), or *s*-triazine, has attracted recent interest due to the unique structure of this molecule, which could be responsible for its symmetric or concerted three-body dissociation mechanism producing three HCN molecules. Ab initio calculations of simple aromatic molecules revealed that the three-body dissociation mechanism is one among possible reaction channels for benzene,[1] pyridine,[2] and pyrimidine.[3] The symmetric three-body decomposition of benzene into three C_2H_2 molecules has a high barrier and cannot play an important role in the dissociation process. Concerted three-molecule dissociation reactions of pyridine ($C_5H_5N \rightarrow 2C_2H_2 + HCN$) and pyrimidine ($C_4H_4N_2 \rightarrow C_2H_2 + 2HCN$) occur through lower barriers and could have observable branching ratios in the overall reaction schemes; however, because several other probable reaction channels producing C_2H_2 and HCN also exist, the investigation of the concerted three-body dissociation reaction appears to be difficult. Infrared fluorescence spectroscopy[4] and mass spectroscopy[5,6] experiments, which were carried out with *s*-triazine, revealed that the nearly exclusive product of its photodissociation is the HCN molecule, which probably results from the three-body dissociation. Ab initio calculations of the ground and excited states of *s*-triazine[7] together with the symmetry analysis revealed that the HCN molecules are the result of the concerted three-body dissociation in the ground state.

The mass spectroscopy experiment with photodissociation of *s*-triazine at two different wavelengths performed by Ondrey and Berson[5] showed that translational energy distributions of the HCN molecules are qualitatively different at 193 and 248 nm. Whereas the translational energy distribution of the HCN fragments at 248 nm has a wide peak near 10 kcal/mol with a long tail toward higher energy values, the distribution at 193 nm has a sharp peak near 2 kcal/mol with a short tail toward higher energies. If we suppose that the *s*-triazine decomposition occurs through the symmetric three-body dissociation mechanism, and so all three fragments have the same translational energy, the total kinetic energy of the fragments at the end of the energy distribution tail at 248 nm appears to be higher than the available energy. Therefore, the HCN moiety observed in the *s*-triazine photodissociation at 248 nm cannot be a result of the symmetric three-body dissociation, but the symmetric process can produce the fragments at 193 nm.

The later experiment on the *s*-triazine photodissociation at different wavelengths performed by Gejo et al.[6] revealed, on the contrary, that the translational energy distributions in the energy interval from 96.9 kcal/mol (295 nm) to 148.1 kcal/mol (193 nm) have similar Gaussian shapes, and the maximum in the distribution shifts from 13.8 to 19.8 kcal/mol when the excitation photon wavelength decreases from 295 to 193 nm. The width of the distribution also increases, especially in the interval from 248 to 193 nm. The translational energy distribution curves obtained at 275, 248, and 193 nm have a Gaussian

† Part of the "Sheng Hsien Lin Festschrift".

* Corresponding author. E-mail: dyakov@pub.iams.sinica.edu.tw.
‡ Institute of Atomic and Molecular Sciences.
§ Florida International University.
|| National Chiao-Tung University.
⊥ National Taiwan University.
National Tsing Hua University.

10.1021/jp0740649 CCC: $37.00
Published on Web 08/28/2007

shape with a long tail toward higher energy values. Alternatively, the 295 and 285 nm curves do not show a high-energy tail. The authors concluded that the *s*-triazine photodissociation is not a symmetric three-body event with simultaneous cleavage of the three bonds, but rather is a sequential process passing through a short-lived $C_2H_2N_2$ intermediate.

In the present Article, we report chemically accurate G3-type calculations of the potential energy surface (PES) for the $C_3H_3N_3$ system, discuss a variety of possible mechanisms of *s*-triazine phododissociation, and compare the experimental data mentioned above with the results obtained by theoretical ab initio and RRKM calculations of rate constants and product branching ratios.

2. Computational Methods

Geometries of all intermediates and transition states in the ground electronic state of $C_3H_3N_3$ were fully optimized using the hybrid density functional B3LYP method[8,9] with the 6-31G* basis set.[10] Connections between transition states and corresponding local minima were confirmed by intrinsic reaction coordinate (IRC) calculations. Optimized geometries of various intermediates and transition states and their total energies are given in the Supporting Information. Energies of intermediates and transition states at B3LYP/6-31G* optimized geometries were calculated using the G3-type computational scheme,[11a] in particular, its G3(MP2,CC)//B3LYP modification.[11b,c] Zero point energy (ZPE) corrections were taken into account using B3LYP/6-31G* frequencies without scaling. All calculations were performed employing the Gaussian 03[12] and MOLPRO 2002[13] program packages. Rice−Ramsperger−Kassel−Marcus (RRKM) and microcanonical variational transition state theories[14−16] have been applied to compute rate constants for individual reaction steps. G3 energies and B3LYP/6-31G* frequencies for all intermediates and transition states were used to perform the RRKM calculations. In these calculations, available internal energy was taken to be equal to the energy of a photon absorbed by the triazine molecule. Relative product yields (branching ratios) were found using the steady-state approach. For the radical product channels, $C_3H_2N_3$ + H, no distinct transition states exist on the PES for the last reaction step, as it is a simple bond cleavage process. In this case, we used the variational transition state theory (VTST)[16] by considering different positions for the transition state along the reaction path, calculating rate constants corresponding to each of them, and finding the minimal rate. Additional computational details of our ab initio/RRKM/VTST approach have been described earlier.[17]

Geometries of excited states of triazine were calculated at the CASSCF/6-31+G* level,[18] where 11 active orbital were occupied by 12 electrons. Energies were then calculated at the MRCI/6-31+G* level,[19] where 10 active orbitals were occupied by 12 electrons. To avoid any restrictions in geometries of transition states and intermediates, we did not use symmetry of molecules in the excited-state calculations.

3. Results and Discussion

Ground-State Dissociation. Main Reaction Channels. The absorption band of *s*-triazine in the excitation range 308−248 nm consists of two transitions:[20,21] $^1A_1 \rightarrow E''$ ($n \rightarrow \pi^*$) and $^1A_1 \rightarrow {}^1A_2$ ($\pi \rightarrow \pi^*$). The absorption band is highly structured, and below 300 nm fluorescence is observed.[20] The existence of fluorescence together with a high electronic excitation energy of HCN indicate that the HCN molecules cannot be a result of excited-state dissociation. HCN is more likely produced from the ground-state dissociation, and so the excited states of triazine formed after absorption of a photon are deactivated by internal conversion and/or intersystem crossing to a lower electronic state.[22] Figure 1 shows PES of the singlet ground state of triazine. To distinguish between reaction channels with the same final products, but via different pathways with different exit barriers, the reaction products in all figures are uniquely denoted depending on the reaction channel in which they are formed; that is, the same product formed through different pathways has different notations. The symmetric three-body dissociation channel via transition state **TS1_P8** has the lowest barrier of 81.0 kcal/mol. The competitive process is the H shift reaction via **TS1_2** followed by a variety of possible ring-opening processes. The reaction through **TS2_3** produces HCN and the $C_2H_2N_2$ (**m54-1**) fragment. Figure 2 shows secondary dissociation reactions of various $C_2H_2N_2$ fragments. The fragment **m54-1** has a low dissociation barrier of 4.5 kcal/mol and can easily decompose into the HCN and HNC moieties. Thus, the dissociation pathway through **TS2_3** presumably initiates sequential reactions, which give two HCN and one HNC fragments. The reaction through **TS2_4** gives the HCN and **m54-2** fragments. The **m54-2** fragment has a very high secondary dissociation barrier (Figure 2), and so, after being produced, it is expected to be detectable in the mass spectra. The reaction through **TS2_P2** is a three-body dissociation reaction, which produces two HCN and one HNC moieties. Yet the reaction barrier of 109.3 kcal/mol seems to be too high to play an important role in the overall dissociation scheme. The reaction pathway through **TS2_5** and **TS5_P4** gives the HNC and $C_2H_2N_2$ (**m54-3**) fragments. The latter (Figure 2) has a dissociation barrier of approximately 40 kcal/mol that looks too high for the secondary dissociation reaction to occur. The reaction channel through **TS2_5** and **TS5_6** produces intermediate **6**, which can decompose to the CH_3N (**m29**) and C_2N_2 (**m52**) fragments by H migration through a barrier at **TS6_8** followed by a single C−N bond cleavage in intermediate **8** occurring without an exit barrier. Dissociation via **TS6_7** and **TS6_P5** does not look to be favorable due to significantly higher reaction barriers. In the RRKM calculations for this channel, we did not take into account the last reaction step, **8** → CH_3N + C_2N_2, and suppose that the C−N bond rupture occurs fast after passing the barrier at **TS6_8**. This assumption is most likely warranted because this process takes place without an exit barrier via a loose variational transition state, the CH_3N + C_2N_2 products are higher in energy than **TS6_8** only by 6.6 kcal/mol, and this energy difference is expected to be compensated by the tight character of the transition state **TS6_8** for the H migration, making the latter the rate-determining step for the production of **m29** + **m52**.

Migration of an H atom above the ring through **TS1_9** followed by HCN elimination producing the **m54-3** fragment has a barrier too high for this channel to play any significant role in the dissociation process. Ring permutation reactions via transition states **TS1_10** and **TS10_11** and Dewar-benzene-like intermediate **10** give 1,2,4-triazine, which in turn can isomerize into 1,2,3-triazine through **TS11_12**, **TS12_13**, and isomer **12**. Dissociation reactions through the 1,2,4-triazine and 1,2,3-triazine isomers have too high dissociation energy to be observed experimentally if the reaction starts from 1,3,5-triazine. H atom elimination reaction, which does not have a distinct transition state, requires 105.9 kcal/mol of energy, 24.9 kcal/mol more than the symmetric three-body dissociation through **TS1_P8**, which makes this reaction unfavorable in comparison with other pathways.

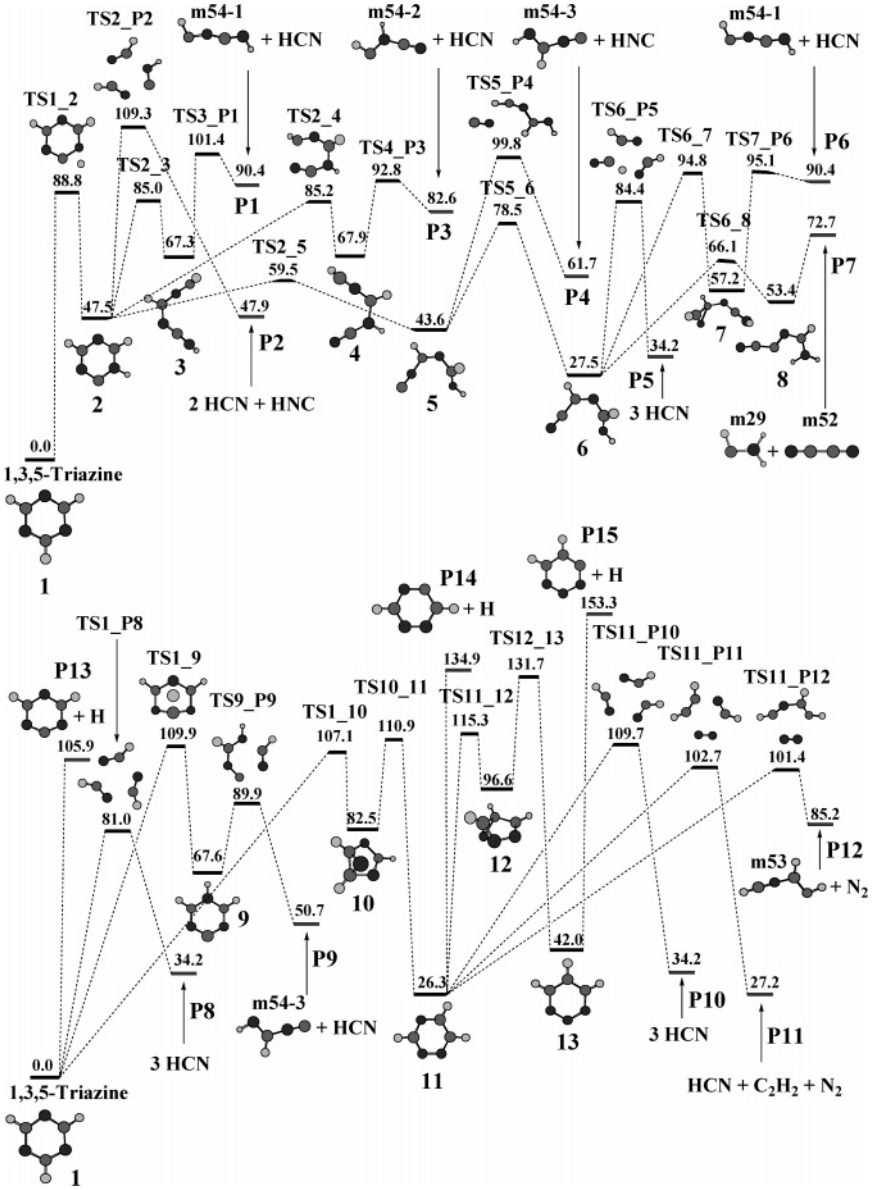

Figure 1. Potential energy surface of 1,3,5-triazine. All energies are given in kcal/mol.

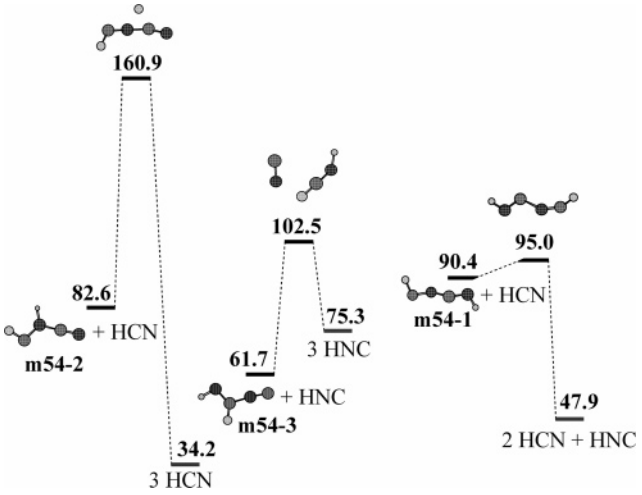

Figure 2. Secondary dissociation reactions of $C_2H_2N_2$ fragments.

RRKM calculations for the reaction channels presented in Figure 1 (the reaction rate constants are given in Table 1) demonstrate that the three-body dissociation reaction through **TS1_P8** is responsible for more than 99% of products in the wide energy range from 295 to 193 nm, so that the HCN molecules should result from the symmetric three-body dissociation, in contradiction to the experimental results.[6]

Opened-Ring Dissociation Pathway. In a series of papers, Zewail et al.[23,24] suggested that an opened-ring diradical isomer plays a major role in photodissociation of the simplest nitrogen-containing aromatic molecules. The opened-ring isomer could be produced as a result of internal conversion from an opened-ring excited-state structure. Figure 3 presents *s*-triazine dissociation pathways through the opened-ring diradical isomer **15**. This isomer is unstable and can easily rearrange into 1,3,5-triazine through a small barrier at **TS1_15**. The geometry and energy of **15** are very close to those of the corresponding triplet state structure. The reactions through **TS15_P17** and **TS15_P18** are two-body dissociation reactions with small exit barriers, which produce HCN and a methastable fragment **m54-4**. The **m54-4** fragment in turn easily decomposes to two HCN molecules via a barrier of approximately 0.1 kcal/mol. The reactions through **TS15_P16** and **TS15_P19** are three-body dissociation reactions with high exit barriers, which produce three HCN molecules. If the photodissociation reaction initiates

TABLE 1: RRKM and VTST Unimolecular Rate Constants (s^{-1}), Reaction Path Degeneracies, and Barrier Heights (kcal/mol) of Various Reaction Steps in Photodissociation of *s*-Triazine via the Ground-State PES Calculated for Different Photon Energies

transition state	reaction	reaction path degeneracy	barriers height, kcal/mol	295 nm 96.9 kcal/mol	285 nm 100.3 kcal/mol	275 nm 104.0 kcal/mol	248 nm 115.3 kcal/mol	193 nm 148.1 kcal/mol	157 nm 182.1 kcal/mol	2 × 275 nm 208.0 kcal/mol	2 × 248 nm 230.6 kcal/mol
VTS1_P13, k_{1_P13}	**1 → P13**	3	105.9				1.2×10^4	9.3×10^7	8.1×10^9	6.3×10^{10}	8.0×10^{10}
TS1_P8, k_{1_P8}	**1 → P8**	1	81.0	6.4×10^6	2.4×10^7	7.9×10^7	1.4×10^9	1.6×10^{11}	2.5×10^{12}	9.8×10^{12}	2.5×10^{13}
TS1_9, k_{1_9}	**1 → 9**	6	109.9					1.7×10^6	2.0×10^8	1.8×10^9	7.2×10^{10}
TS1_9, k_{-1_9}	**9 → 1**	2	109.9					7.6×10^8	1.4×10^{10}	5.0×10^{10}	1.0×10^{11}
TS9_P9, k_{9_P9}	**9 → P9**	2	89.9					2.9×10^{12}	1.1×10^{13}	2.0×10^{13}	2.8×10^{13}
TS1_10, k_{1_10}	**1 → 10**	6	107.1					3.3×10^6	2.6×10^8	2.1×10^9	8.4×10^9
TS1_10, k_{-1_10}	**10 → 1**	1	107.1					5.5×10^{10}	3.5×10^{11}	7.7×10^{11}	1.2×10^{12}
TS10_11, k_{10_11}	**10 → 11**	2	110.9					9.1×10^{10}	9.2×10^{11}	2.4×10^{12}	4.4×10^{12}
TS10_11, k_{-10_11}	**11 → 10**	2	110.9					1.4×10^7	1.0×10^9	7.2×10^9	2.6×10^{10}
TS11_P12, k_{11_P12}	**11 → P12**	1	101.4					1.4×10^{10}	5.8×10^{11}	3.3×10^{12}	9.9×10^{12}
TS11_P11, k_{11_P11}	**11 → P11**	1	102.7					2.9×10^{10}	1.4×10^{12}	8.1×10^{12}	2.5×10^{13}
TS11_P10, k_{11_P10}	**11 → P10**	1	109.7					6.5×10^9	6.5×10^{11}	5.1×10^{12}	1.9×10^{13}
TS1_2, k_{1_2}	**1 → 2**	6	88.8	7.2×10^3	4.0×10^4	1.9×10^5	5.8×10^6	1.4×10^9	3.0×10^{10}	1.4×10^{11}	4.0×10^{11}
TS1_2, k_{-1_2}	**2 → 1**	1	88.8	2.8×10^6	1.1×10^7	3.9×10^7	5.3×10^8	2.5×10^{10}	1.8×10^{11}	4.5×10^{11}	8.3×10^{11}
TS2_5, k_{2_5}	**2 → 5**	2	59.5	2.5×10^{12}	3.0×10^{12}	3.5×10^{12}	5.4×10^{12}	1.2×10^{13}	1.8×10^{13}	2.3×10^{13}	2.8×10^{13}
TS2_5, k_{-2_5}	**5 → 2**	1	59.5	8.3×10^9	1.0×10^{10}	1.2×10^{10}	2.0×10^{10}	4.9×10^{10}	8.3×10^{10}	1.1×10^{11}	1.3×10^{11}
TS5_P4, k_{5_P4}	**5 → P4**	1	99.8		7.9×10^1	7.8×10^4	8.2×10^7	9.5×10^{10}	2.0×10^{12}	8.3×10^{12}	2.0×10^{13}
TS5_6, k_{5_6}	**5 → 6**	2	78.5	5.0×10^8	1.1×10^9	2.3×10^9	1.2×10^{10}	1.8×10^{11}	7.5×10^{11}	1.5×10^{12}	2.4×10^{12}
TS5_6, k_{-5_6}	**6 → 5**	2	78.5	3.2×10^7	8.0×10^7	2.0×10^8	1.5×10^9	4.2×10^{10}	2.8×10^{11}	7.1×10^{11}	1.3×10^{12}
TS6_7, k_{6_7}	**6 → 7**	1	94.8	1.5×10^1	3.2×10^2	3.1×10^3	2.4×10^5	9.1×10^7	1.7×10^9	6.9×10^9	1.7×10^{10}
TS6_7, k_{-6_7}	**7 → 6**	1	94.8	8.1×10^3	1.2×10^5	8.8×10^5	3.1×10^7	2.7×10^9	2.0×10^{10}	5.2×10^{10}	9.3×10^{10}
TS7_P6, k_{7_P6}	**7 → P6**	1	95.1	2.7×10^4	1.1×10^6	1.2×10^7	8.0×10^8	1.1×10^{11}	9.5×10^{11}	2.6×10^{12}	4.8×10^{12}
TS6_P5, k_{6_P5}	**6 → P5**	1	84.4	8.9×10^5	3.7×10^6	1.3×10^7	2.4×10^8	2.3×10^{10}	2.5×10^{11}	8.2×10^{11}	1.8×10^{12}
TS6_8, k_{6_8}	**6 → 8 (P7)**	1	66.1	5.8×10^8	9.6×10^8	1.6×10^9	5.3×10^9	4.9×10^{10}	1.8×10^{11}	3.5×10^{11}	5.5×10^{11}
TS2_4, k_{2_4}	**2 → 4**	2	85.2	8.1×10^7	2.5×10^8	6.8×10^8	6.2×10^9	1.8×10^{11}	9.7×10^{11}	2.2×10^{12}	3.8×10^{12}
TS2_4, k_{-2_4}	**4 → 2**	1	85.2	8.2×10^7	1.7×10^8	3.2×10^8	1.2×10^9	7.4×10^9	1.8×10^{10}	2.6×10^{10}	3.4×10^{10}
TS4_P3, k_{4_P3}	**4 → P3**	1	92.8	5.3×10^6	4.8×10^7	2.4×10^8	4.4×10^9	1.4×10^{11}	6.0×10^{11}	1.2×10^{12}	1.8×10^{12}
TS2_3, k_{2_3}	**2 → 3**	2	85.0	6.6×10^7	2.0×10^8	5.2×10^8	4.6×10^9	1.3×10^{11}	6.9×10^{11}	1.6×10^{12}	2.6×10^{12}
TS2_3, k_{-2_3}	**3 → 2**	1	85.0	1.6×10^8	3.2×10^8	6.1×10^8	5.0×10^9	1.4×10^{10}	3.4×10^{10}	5.1×10^{10}	6.5×10^{10}
TS2_P2, k_{2_P2}	**2 → P2**	1	109.3					4.4×10^{10}	2.4×10^{12}	1.4×10^{13}	4.0×10^{13}
TS3_P1, k_{3_P1}	**3 → P1**	1	101.4			1.3×10^5	2.3×10^8	1.0×10^{11}	1.0×10^{12}	2.9×10^{12}	5.4×10^{12}
TS1_14, k_{1_14}	**1 → 14**	12	104.3				1.0×10^5	1.6×10^9	1.1×10^{11}	8.3×10^{11}	3.2×10^{12}
TS1_14, k_{-1_14}	**14 → 1**	2	104.3				1.1×10^9	6.9×10^{11}	8.3×10^{13}	2.5×10^{13}	4.8×10^{13}
TS14_15, k_{14_15}	**14 → 15**	2	105.1				6.4×10^8	5.4×10^{11}	7.0×10^{12}	7.0×10^{12}	4.2×10^{13}
TS14_15, k_{-14_15}	**15 → 14**	1	105.1				1.9×10^{12}	2.0×10^{12}	2.1×10^{12}	2.1×10^{12}	2.1×10^{12}
TS1_15, k_{1_15}	**1 → 15**	12	106.0				3.4×10^4	9.1×10^8	8.3×10^{10}	7.0×10^{11}	2.8×10^{12}
TS1_15, k_{-1_15}	**15 → 1**	1	106.0				1.0×10^{12}	1.7×10^{12}	2.0×10^{12}	2.1×10^{12}	2.1×10^{12}
TS15_P16, k_{15_P16}	**15 → P16**	1	109.1				1.5×10^{11}	3.2×10^{12}	6.4×10^{12}	8.4×10^{12}	9.8×10^{12}
TS15_P17, k_{15_P17}	**15 → P17**	1	120.4					2.3×10^{11}	2.3×10^{12}	5.0×10^{12}	7.8×10^{12}
TS15_P18, k_{15_P18}	**15 → P18**	1	124.2					3.2×10^{10}	6.4×10^{11}	1.7×10^{12}	3.1×10^{12}
TS15_P19, k_{15_P19}	**15 → P19**	1	126.0					1.9×10^{10}	6.2×10^{11}	1.9×10^{12}	1.9×10^{12}

from the most stable isomer **1**, the ring-opening reaction cannot play an important role because of high barriers. However, if the reaction starts from the opened-ring isomer **15**, the branching ratios of the reaction pathways through opened-ring transition states **TS15_P16**, **TS15_P17**, **TS15_P18**, and **TS15_P19** become significant at 193 nm (see Table 2). At 248 nm, only the route via the transition state **TS15_P16** has an observable branching ratio; the other transition states lie above the photon energy. All reactions going through the diradical transition states **TS15_P16**, **TS15_P17**, **TS15_P18**, and **TS15_P19** are not symmetric and can provide some fragments with higher translational energy. This reaction scheme is in good agreement with the experimental translational energy distributions of the HCN moiety.[6] Branching ratios of the HCN molecules produced via the diradical transition states increase when the photon energy grows, and this can be responsible for the high-energy tail in the translational energy distributions observed at 248 and 193 nm. The 275 nm distribution also has a small high-energy tail, although the photon energy (104 kcal/mol) is somewhat lower than the energy required to overtake the barrier at **TS15_P16** (109.1 kcal/mol). However, it should be mentioned that G3 calculations for open-shell singlet structures like isomer **15** and transition states **TS15_P16**, **TS15_P17**, **TS15_P18**, and **TS15_P19** may not be very accurate, so that the energy for the structures **15** and **TS15_P16** can be overestimated. This means that some fraction of the HCN fragments might be produced through the barrier at **TS15_P16** even in the 275 nm experiments.

The part of HCN molecules, which is produced through isomerization into the most stable ring isomer **1**, can be responsible for the Gaussian-shaped section of the distribution. In the 285 nm (100.3 kcal/mol) and 295 nm (96.9 kcal/mol) experiments, the translational energy distribution curves have a Gaussian shape and almost reach zero at 30 kcal/mol. If the symmetric three-body dissociation mechanism is supposed for these two experiments, the sum of translational energies of all three fragments at the upper limit of the distribution should be equal to 90 kcal/mol, which is more than the difference between the photon energy (100.3 or 96.9 kcal/mol) and the energy of the products (34.2 kcal/mol). Yet because of the high internal energy acquired by *s*-triazine, the D_{3h} symmetry of the molecule can be distorted by intramolecular vibrations. Hence, the three-body dissociation through the symmetric channel via **TS1_P8** may not be completely symmetric, and different HCN moieties can have slightly different translational energies even if the reaction occurs via the symmetric transition state. At high energies of the absorbed photon, the dissociation through the diradical transition states is likely to become dominant.

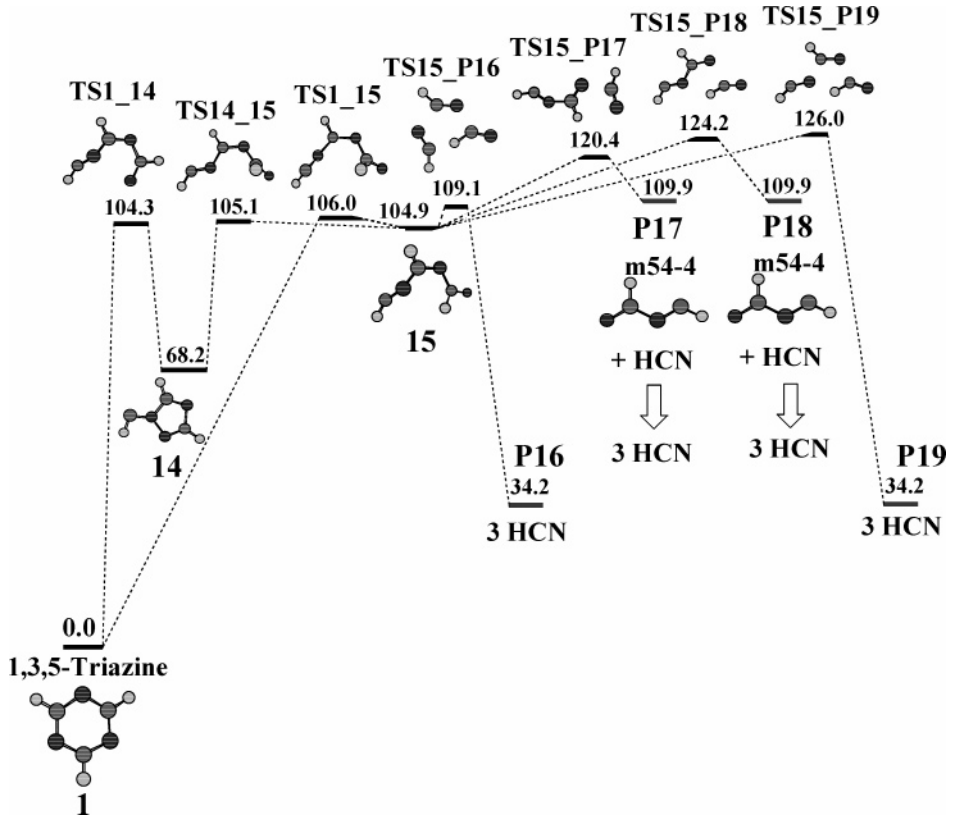

Figure 3. *s*-Triazine dissociation pathways starting from the opened-ring isomer **15**.

TABLE 2: Product Branching Ratios (%) in *s*-Triazine Photodissociation at Different Photon Energies[a]

		energy (wavelength)														
		115.3 kcal/mol (248 nm)			148.1 kcal/mol (193 nm)			182.1 kcal/mol (157 nm)			208.0 kcal/mol (2 × 275 nm)			230.6 kcal/mol (2 × 248 nm)		
products		**1**	**2**	**15**	**1**	**2**	**15**	**1**	**2**	**15**	**1**	**2**	**15**	**1**	**2**	**15**
P1	HCN + $C_2H_2N_2$ (**m54-1**)					1.1			3.0			3.9			3.5	
P2	2HCN + HNC					0.4		0.1	11.1		0.4	34.1		0.7	53.4	
P3	HCN + $C_2H_2N_2$ (**m54-2**)		0.3			1.7		0.3	4.4	0.1	0.3	5.3	0.1	0.3	5.0	
P4	HCN + $C_2H_2N_2$ (**m54-3**)		0.9		0.4	43.9	0.2	0.6	65.6	0.2	0.6	50.0	0.1	0.5	34.5	
P5	3HCN		4.3		0.1	16.8			8.9			4.0			2.1	
P7	CH_3N (**m29**) + C_2N_2 (**m52**)	0.4	94.5	0.4	0.3	35.8	0.2		6.2			1.7			0.6	
P8	3HCN (symmetric 3-body)	99.6		93.2	98.7	0.3	44.1	96.0	0.8	27.2	91.3	1.0	16.5	85.2	0.9	10.7
P13	H + $C_3H_2N_3$							0.3		0.1	0.6		0.1	0.3		
P16	3HCN			6.4	0.5		51.0	1.7		46.5	3.3		41.1	5.6		38.7
P17	3HCN						3.7	0.6		16.7	2.0		24.5	4.5		30.8
P18	3HCN						0.5	0.2		4.7	0.7		8.3	1.8		12.3
P19	3HCN						0.3	0.2		4.5	0.8		9.3	1.1		7.5

[a] Reaction initiates from three possible structures: isomer **1**, isomer **2**, and isomer **15**.

In the experimental results reported by Ondrey and Bersohn,[5] the translational energy distribution at 193 nm has a shape similar to the Gaussian distribution function without a high-energy tail and with a maximum near zero. Later experiments reported by Gejo et al.[6] revealed the Gaussian shape only when low-energy photons (285 and 295 nm) were used, which initiate symmetric three-body dissociation. Yet the maximum of the distributions at 285 and 295 nm was observed near the value of 13 kcal/mol. At 193 nm, the distribution[6] becomes spread in both directions: toward zero on one side and toward the high-energy limit on the other. As was mentioned above, this is likely a superposition of two different reactions: one initiates from the ring isomer **1**, and the other starts from diradical isomer **15**. We could suppose that the distribution function at 193 nm from the experiment of Ondrey and Bersohn[5] is entirely a result of the reaction initiated from ring isomer **1**. It is difficult to predict the shape of the distribution if only the symmetric three-body dissociation reaction is observed, and dynamics calculations are most appropriate for this purpose. However, the extremely high amount of internal energy can result in non-equilibrium behavior, which can redistribute internal energy of the parent molecule in favor of internal energy of fragments instead of translational energy. Therefore, it is possible that photodissociation by higher-energy photons, if it starts from isomer **1**, may favor lower translational energy of the fragments.

Dissociation via H Atom Shift. If we disengage ourselves for now from the discussion about the excited-state isomerization mechanism, which could occur after photon absorption but before internal conversion into the ground electronic state, another one-step reaction can be suggested, in which an H atom migrates from C to N to produce isomer **2**. In Table 2, we show dissociation product branching ratios calculated with the assumption that the reaction starts from the energized isomer **2**. One can see that in this case the symmetric three-body

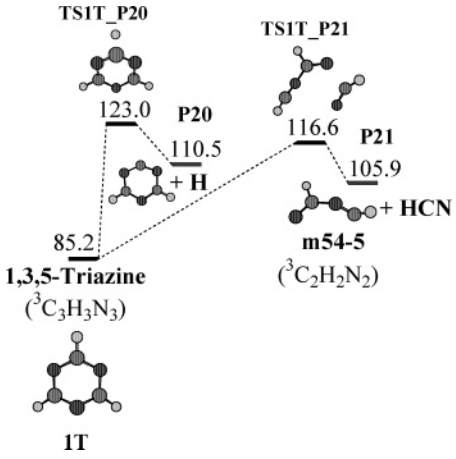

Figure 4. PES of *s*-triazine in the lowest triplet state.

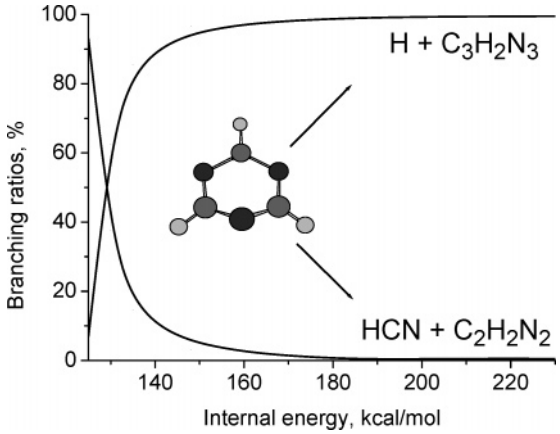

Figure 5. Branching ratios of products of the lowest triplet state dissociation.

dissociation channel through **TS1_P8** has a very low branching ratio. The major products are the **m54-3**, HNC, CH_3N, and C_2N_2 moieties. At high energies, the branching ratio of the **m54-2** fragment also becomes significant. The **m54-2** and **m54-3** fragments have high barriers for secondary dissociation (see Figure 2) and could be easily detected. However, because only the HCN (or HNC) molecule was observed in the experimental mass spectra,[4−6] we can conclude that the dissociation of *s*-triazine on the ground-state PES following photoexcitation and internal conversion is unlikely to start from isomer **2**.

Dissociation in the Lowest Triplet State. In Figure 4, we present the potential energy surface of the dissociation reaction from the first triplet state, which can occur after intersystem crossing from an excited singlet state. The main dissociation channels, $^3C_3H_3N_3 \rightarrow {}^3C_2H_2N_2 + HCN$ and $^3C_3H_3N_3 \rightarrow {}^3C_3H_2N_3 + H$, exhibit barriers above or just near the energy of 248 nm photons. So, these reactions cannot be observed at 295, 285, and 275 nm. Being the dominant product in the narrow energy interval just above 123 kcal/mol, the HCN elimination channel becomes minor at higher energies. Above 180 kcal/mol, only the H atom elimination reaction can be observed (see Figure 5 and Table 3). So, the role of the first triplet state dissociation seems to be insignificant due to high energies of the products and judging from the large difference of the calculated product yields in comparison with the experimental data.

Excited-State Isomerization. By applying the MRCI/6-31+G* ab initio calculations to evaluate vertical excitation energies, we found for the lowest triplet (T_1) and singlet (S_1, S_2, S_3, S_4) excited states the values of 109.6, 125.6, 130.2, 138.3, and 194.9 kcal/mol, respectively. The first three singlet excited states, which, according to our calculations, all correspond to $\pi \rightarrow \pi^*$ transitions, respectively, have rather similar vertical energies, but the potential energy surface of the S_1 state is quite different from the other excited states (see Figure 6); S_4 has a mixed σ-π^*/n-π^* character. The energy of the first excited state, being optimized, decreases dramatically to the value of 96.6 kcal/mol, which is close to the relative energy of the lowest triplet state T_1. On the contrary, energies of the other excited states at the S_1-optimized geometry are significantly higher than their vertical values. If one of the C−N distances increases, the energy of the first excited state increases, and at the distance of 2.0 Å reaches a maximum value of 118.9 kcal/mol, which is lower than the vertical excitation energy. After crossing over a barrier, the system relaxes to the opened-ring structure **15_ex** similar to the structure **15** on the ground-state PES. The energies of the S_1 and S_0 states at the opened-ring geometry are very close, which indicates an existence of a crossing point or a conical intersection between these two states, which should facilitate $S_1 \rightarrow S_0$ internal conversion. We had difficulties with calculations of the exact geometry and energy of the opened-ring structure in the S_1 state because of poor convergence of the wavefunction, typical for the vicinity of a structure where two different PES's cross each other. We obtained the energy of 109.9 kcal/mol for the optimized structure **15_ex** in the S_1 state. Geometry optimization starting from the geometry of **15_ex** in the ground electronic state converged to the opened-ring structure **15**.

The value of 109.1 kcal/mol was computed for the structure **15_ex** in the ground electronic S_0 state. This result is higher than the G3 energy (104.9 kcal/mol) of isomer **15** (Figure 3). In general, the present MRCI calculations with a limited active space reproduce well qualitative behavior of the wavefunction, but tend to overestimate excited-state energies, especially for nonequilibrium strained structures and, in particular, the vertical excitation energies. So, in reality these energies can be somewhat lower, and the difference between the vertical and adiabatic excitation energies of S_1 may be smaller. To explain the different behavior of the translational energy distributions at 295 and 285 nm, on one hand, and at 275, 248, and 193 nm, on the other, we can suppose that after excitation by 295 or 285 nm photons to the first excited state, the molecule does not have enough energy to overcome the barrier at the **TS1_ex** transition state on the S_1 PES. If a 275, 248, or 193 nm photon is absorbed, the energy is sufficient to overcome the barrier, and the molecule isomerizes to the opened-ring structure **15_ex** followed by internal conversion to structure **15** in the ground electronic state.

The second excited state S_2 also exhibits a barrier toward the opened-ring structure **15_ex′** (see Figure 6a and b), but this barrier, nearly 150 kcal/mol, is much higher than that for the

TABLE 3: RRKM Unimolecular Rate Constants (s^{-1}) and Reaction Path Degeneracies of Various Reaction Steps in Photodissociation of *s*-Triazine Calculated for Different Photon Energies on the First Triplet State PES

	transition state/reaction/ reaction path degeneracy	
energy, kcal/mol	**TS1T_P20**, k_{1T_P20}/ **1T → P20**/6	**TS1T_P21**, k_{1T_P21}/ **1T → P21**/6
125.0	9.0×10^6	1.2×10^8
130.0	1.2×10^9	7.2×10^8
135.0	1.7×10^{10}	2.9×10^9
148.1 (193 nm)	8.7×10^{11}	3.0×10^{10}
182.1 (157 nm)	6.9×10^{13}	6.3×10^{11}
208.1 (2 × 275 nm)	3.5×10^{14}	2.1×10^{12}
230.6 (2 × 248 nm)	8.8×10^{14}	4.4×10^{12}

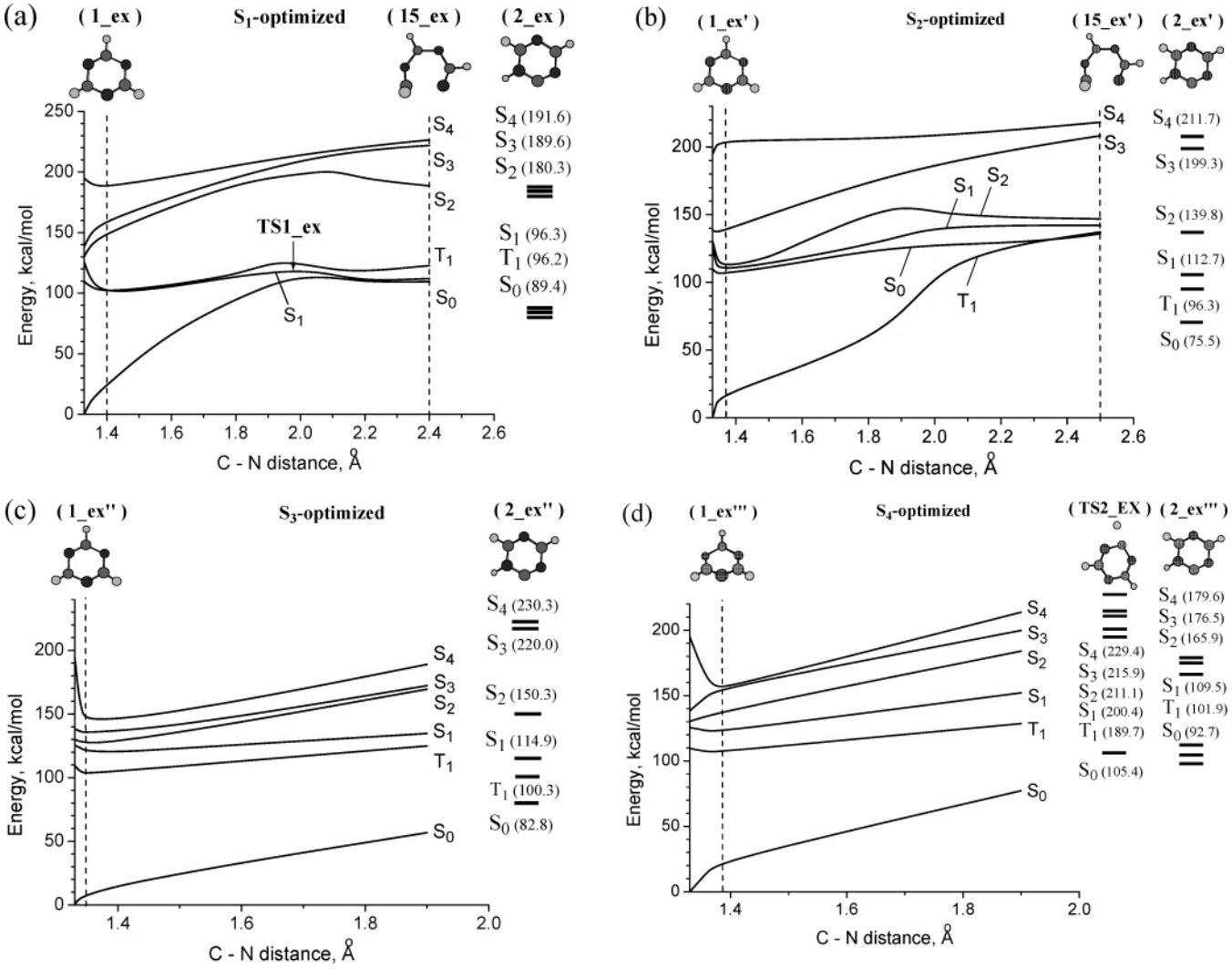

Figure 6. Ring-opening reaction on the excited-state potential energy surfaces of triazine. One of the C−N distances is fixed; all other distances and angles are optimized for the S_1 (a), S_2 (b), S_3 (c), and S_4 (d) excited states. The dashed line on the left corresponds to the optimized geometry of the appropriate excited state. In addition, the energy levels of the H-shifted isomer **2_ex** at the geometries optimized for the appropriate excited state are given on the right. Part (d) also includes the energy levels for the structure **TS2_EX**, corresponding to the transition state between isomers **1_ex** and **2_ex** on the S_4 PES. Geometry optimization of all structures was performed at the CASSCF/6-31+G* level; energies of the optimized structures then were recalculated by the MRCI/6-31+G* method.

first excited state, and approximately equal to the energy of 193 nm photons. The energy gap between S_1 and S_2 states at the opened-ring geometry is small, which indicates an existence of a crossing point or a conical intersection between these two states, as it is the case at the opened-ring geometry **15_ex** on the S_1 PES. On the other hand, the S_2 PES shows another conical intersection (or an avoided crossing point) with the PES of S_1 near the global minimum of the S_2 state, which has configuration very close to the closed-ring structure **1**. The existence of the conical intersections means that under certain conditions internal conversion $S_2 \rightarrow S_1$ can occur both at the opened-ring geometry **15_ex′** and at the ring geometry **1_ex′**, followed by internal conversion into the ground-state structures **15** or **1**, respectively. We can suppose that if the energy of the excitation photon is not high enough to overtake the barrier on the S_2 PES, the molecule relaxes to the global closed-ring minimum **1_ex′** on the S_2 PES, followed by two-step internal convergence into S_1, and then into S_0. If the photon energy is sufficient for crossing over the barrier, the molecule can isomerize into the structure **15_ex′**, followed by the internal convergence into the opened-ring structure **15_ex** on the S_1 PES, and then into the structure **15** on the ground-state PES.

We could not find any transition states for the C−N bond cleavage in the S_3 and S_4 excited states. Even if such transition states exist, they should have extremely high energies. However, in the vicinity of equilibrium structures on the PES, the S_3 state is likely to have a crossing point with the S_2 state, and the S_4 surface may cross with the S_3 surface (see Figure 6c and d). This is supported by CASSCF calculations, which reveal very small energy gaps both between S_4 and S_3 and between S_3 and S_2: 175.8 versus 175.7 kcal/mol, and 133.0 versus 132.3 kcal/mol, respectively. MRCI calculations performed at the same geometries give 156.4 versus 155.7 kcal/mol and 135.3 versus 125.1 kcal/mol for the S_4-S_3 and S_3-S_2 pairs, respectively. The difference in the CASSCF and MRCI values of the gap can be attributed to the fact that the size of the energy gap between different electronic states is very sensitive to small changes in geometry in the vicinity of the crossing point. Meanwhile, the existence of the S_4-S_3 and S_3-S_2 crossing points at the CASSCF level indicates they are likely to be also found at the higher MRCI level and to exist in reality. Therefore, the sequential relaxation $S_3 \rightarrow S_2 \rightarrow S_1 \rightarrow S_0$ and $S_4 \rightarrow S_3 \rightarrow S_2 \rightarrow S_1 \rightarrow S_0$ (cascade internal conversion) from S_3 and S_4 into

the ground state leading to the formation of the energized isomer **1** should be feasible.

Also, we were not able to locate any transition state for the hydrogen shift reaction on the S_1, S_2, and S_3 excited surfaces. For all of these states, a change in the position of the H atom leads to configurations with very high energies. For the S_4 state, we found a structure **TS2_EX**, which seems to be a transition state between the structures **1_ex‴** and **2_ex‴**. However, the calculated barrier height of 229.4 kcal/mol makes this isomerization channel possible only upon excitation by high-energy photons.

Summarizing, depending on the available internal energy acquired by the *s*-triazine molecule through photoexcitation and on the particular electronic state it is excited to, internal conversion back to the ground S_0 state can occur either in the vicinity of the ring isomer **1** or at the opened-ring geometry close to the structure **15**. This would control the initial geometry in ground electronic state from which the dissociation reaction starts and thus affect branching ratios of various dissociation channels and the shape of translational energy distributions of the products. So, according to the photon energy and experimental conditions, we can distinguish five different scenarios of the isomerization mechanism involving the first four excited states (in the present Article we do not discuss higher excited states).

(1) Excitation occurs to the lowest excited state S_1, but the photon energy is not sufficient for overtaking the C−N bond cleavage barrier on the S_1 PES. In this case, the system relaxes to the ring isomer **1** on the ground-state PES by internal conversion, and dissociation initiates from the isomer **1**. Next, all HCN molecules are produced by the symmetric three-body dissociation reaction.

(2) Excitation occurs to the lowest excited state S_1, and the photon energy is enough to cross over the barrier on the S_1 PES. In this case, the molecule can isomerize to the opened-ring isomer **15_ex** on the S_1 surface, which is followed by internal conversion to the opened-ring ground-state isomer **15**. The HCN moieties can then be formed through both the symmetric three-body channel and two-body sequential dissociation reactions. The translational energy distribution in this case may show a tail toward high-energy values.

(3) Excitation occurs to the S_2 excited state, but the available energy is too low to overcome the isomerization barrier on the S_2 PES. In this case, the system relaxes to the ground electronic state in the vicinity of the adiabatic minimum **1_ex′** on the S_2 PES through the $S_2 \rightarrow S_1 \rightarrow S_0$ route. The dissociation reaction initiates from the ring isomer **1**, as in case (1), but with higher available internal energy.

(4) Excitation occurs to the S_2 excited state, and the available energy is sufficient to pass over the barrier on the S_2 PES and reach another crossing point in the vicinity of **15_ex′**. Internal conversion $S_2 \rightarrow S_0$ or $S_2 \rightarrow S_1 \rightarrow S_0$ at this geometry leads to relaxation into the opened-ring geometry **15**, and then to dissociation through the same mechanism as in case (2), but with higher internal energy.

(5) Excitation takes place to the higher electronic levels S_3 or S_4. Because no low-energy transition states for ring opening were found on the S_3 and S_4 PES, the molecule relaxes to the ground state through cascade internal conversion $S_3 \rightarrow S_2 \rightarrow S_1 \rightarrow S_0$ or $S_4 \rightarrow S_3 \rightarrow S_2 \rightarrow S_1 \rightarrow S_0$ in the vicinity of the closed-ring minimuma **1_ex″** and **1_ex‴**. This relaxation mechanism produces the ring isomer **1**, as in cases (1) and (3), but with much higher internal energy. This photodissociation mechanism can be responsible for a very narrow translational energy distribution with a maximun near zero, which can be a result of ultrafast nonequilibrium decay of the hot molecule, as was mentioned above.

4. Conclusions

The present ab initio and RRKM calculations reveal that there exist two possible dissociation mechanisms of 1,3,5-triazine, and both of them can be observed in experiment. The first is a reaction initiating from the ring isomer **1** (the most stable isomer of 1,3,5-triazine). This reaction occurs through the symmetric three-body dissociation mechanism and gives a Gaussian shape of the translational energy distribution of the HCN moieties. The second mechanism is the reaction starting from the opened-ring isomer **15** and generating a wide translational energy distribution with a long tail toward high-energy values. This is a result of the isomerization ring-opening process in the excited electronic state followed by internal conversion into the ground-state diradical isomer **15**. If the photon energy is not sufficient for the excited-state isomerization, as in the cases of 285 and 295 nm photons, the molecule relaxes into the closed-ring isomer **1** and the symmetric three-body dissociation ensues. However, if the photoexcited molecule possesses enough energy for the excited-state isomerization, as it does at 275, 248, or 193 nm photodissociation, the internal conversion can occur into the opened-ring structure **15**, and the dissociation through various non-symmetric pathways follows.

Acknowledgment. This work was supported in part by Academia Sinica and the National Science Council of Taiwan, R.O.C., and by the Chemical Sciences, Geosciences and Biosciences Division, Office of Basic Energy Sciences, Office of Sciences of U.S. Department of Energy (Grant No. DE-FG02-04ER15570) at FIU.

Supporting Information Available: Optimized Cartesian coordinates of all species involved in the 1,3,5-triazine isomerization and dissociation reactions, and their total energies including ZPE calculated at the B3LYP/6-31G* level of theory. This material is available free of charge via the Internet at http://pubs.acs.org.

References and Notes

(1) Kislov, V. V.; Nguyen, T. L.; Mebel, A. M.; Lin, S. H.; Smith, S. C. *J. Chem. Phys.* **2004**, *120*, 7008.

(2) Lin, M. F.; Dyakov, Y. A.; Tseng, C. M.; Mebel, A. M.; Lin, S. H.; Lee, Y. T.; Ni, C. K. *J. Chem. Phys.* **2005**, *123*, Art. No. 054309.

(3) Lin, M. F.; Dyakov, Y. A.; Tseng, C. M.; Mebel, A. M.; Lin, S. H.; Lee, Y. T.; Ni, C. K. *J. Chem. Phys.* **2006**, *124*, Art. No. 084303.

(4) Goates, S. R.; Chu, J. O.; Flynn, G. W. *J. Chem. Phys*. **1984**, *81*, 4521.

(5) Ondrey, G. S.; Bersohn, R. *J. Chem. Phys*. **1984**, *81*, 4517.

(6) Gejo, T.; Harrison, J. A.; Huber, J. R. *J. Phys. Chem*. **1996**, *100*, 13941.

(7) Osamura, Y.; Unno, M.; Hashimoto, K. *J. Am. Chem. Soc*. **1987**, *109*, 1370.

(8) (a) Becke, A. D. *J. Chem. Phys*. **1992**, *96*, 2155. (b) Becke, A. D. *J. Chem. Phys*. **1992**, *97*, 9173. (c) Becke, A. D. *J. Chem. Phys*. **1993**, *98*, 5648.

(9) Lee, C.; Yang, W.; Parr, R. G. *Phys. Rev*. **1988**, *B37*, 785.

(10) Hehre, W. J.; Ditchfield, R.; Pople, J. A. *J. Chem. Phys.* **1972**, *56*, 2257.

(11) (a) Curtiss, L. A.; Raghavachari, K.; Redfern, P. C.; Rassolov, V.; Pople, J. A. *J. Chem. Phys.* **1998**, *109*, 7764. (b) Baboul, A. G.; Curtiss, L. A.; Redfern, P. C.; Raghavachari, K. *J. Chem. Phys.* **1999**, *110*, 7650. (c) Curtiss, L. A.; Raghavachari, K.; Redfern, P. C.; Baboul, A. G.; Pople, J. A. *Chem. Phys. Lett.* **1999**, *314*, 101.

(12) Frisch, M. J.; Trucks, G. W.; Schlegel, H. B.; Scuseria, G. E.; Robb, M. A.; Cheeseman, J. R.; Montgomery, J. A., Jr.; Vreven, T.; Kudin, K. N.; Burant, J. C.; Millam, J. M.; Iyengar, S. S.; Tomasi, J.; Barone, V.; Mennucci, B.; Cossi, M.; Scalmani, G.; Rega, N.; Petersson, G. A.;

Nakatsuji, H.; Hada, M.; Ehara, M.; Toyota, K.; Fukuda, R.; Hasegawa, J.; Ishida, M.; Nakajima, T.; Honda, Y.; Kitao, O.; Nakai, H.; Klene, M.; Li, X.; Knox, J. E.; Hratchian, H. P.; Cross, J. B.; Bakken, V.; Adamo, C.; Jaramillo, J.; Gomperts, R.; Stratmann, R. E.; Yazyev, O.; Austin, A. J.; Cammi, R.; Pomelli, C.; Ochterski, J. W.; Ayala, P. Y.; Morokuma, K.; Voth, G. A.; Salvador, P.; Dannenberg, J. J.; Zakrzewski, V. G.; Dapprich, S.; Daniels, A. D.; Strain, M. C.; Farkas, O.; Malick, D. K.; Rabuck, A. D.; Raghavachari, K.; Foresman, J. B.; Ortiz, J. V.; Cui, Q.; Baboul, A. G.; Clifford, S.; Cioslowski, J.; Stefanov, B. B.; Liu, G.; Liashenko, A.; Piskorz, P.; Komaromi, I.; Martin, R. L.; Fox, D. J.; Keith, T.; Al-Laham, M. A.; Peng, C. Y.; Nanayakkara, A.; Challacombe, M.; Gill, P. M. W.; Johnson, B.; Chen, W.; Wong, M. W.; Gonzalez, C.; Pople, J. A. *Gaussian 03*, revision C.02; Gaussian, Inc.: Wallingford, CT, 2004.

(13) MOLPRO is a package of ab initio programs written by H.-J. Werner and P. J. Knowles with contributions from Almlöf, J.; Amos, R. D.; Deegan, M. J. O.; Elbert, S. T.; Hampel, C.; Meyer, W.; Peterson, K.; Pitzer, R.; Stone, A. J.; Taylor, P. R.; and Lindh, R.

(14) Eyring, H.; Lin, S. H.; Lin, S. M. *Basic Chemical Kinetics*; Wiley: New York, 1980.

(15) Robinson, P. J.; Holbrook, K. A. *Unimolecular Reactions*; Wiley: New York, 1972.

(16) Steinfeld, J. I.; Francisco, J. S.; Hase, W. L. *Chemical Kinetics and Dynamics*; Prentice Hall: New Jersey, 1999.

(17) Dyakov, Y. A.; Ni, C. K.; Lin, S. H.; Lee, Y. T.; Mebel, A. M. *J. Phys. Chem. A* **2005**, *109*, 8774.

(18) (a) Werner, H.-J.; Knowles, P. J. *J. Chem. Phys.* **1985**, *82*, 5053. (b) Knowles, P. J.; Werner, H. J. *Chem. Phys. Lett.* **1985**, *115*, 259.

(19) (a) Werner, H.-J.; Knowles, P. J. *J. Chem. Phys.* **1988**, *89*, 5803. (b) Knowles, P.-J.; Werner, H. J. *Chem. Phys. Lett.* **1988**, *145*, 514.

(20) Bolovinos, A.; Tsekeris, P.; Philis, J.; Pantos, E.; Andritsopoulos, G. *J. Mol. Spectrosc.* **1984**, *103*, 240.

(21) Innes, K. K.; Ross, I. G.; Moomaw, W. R. *J. Mol. Spectrosc.* **1988**, *132*, 492.

(22) Saigusa, H.; Lim, E. C. *J. Chem. Phys.* **1983**, *78*, 91.

(23) Zhong, D.; Diau, E. W.-G.; Bernhardt, T. M.; Feyter, S. D.; Roberts, J. D.; Zewail, A. H. *Chem. Phys. Lett.* **1998**, *298*, 129.

(24) Lobastov, V. A.; Srinivasan, R.; Goodson, B. M.; Ruan, C. Y.; Feenstra, J. S.; Zewail, A. H. *J. Phys. Chem. A* **2001**, *105*, 11159.